

Original article

DOI: <https://doi.org/10.18721/JPM.17207>

## TRANSFORMATION OF THE STRUCTURE OF THIN METAL FILMS UPON ACTIVATION OF THEIR ABILITY TO LOW-VOLTAGE ELECTRON EMISSION

*I. S. Bizyaev<sup>1</sup>, P. A. Karaseov<sup>1</sup>, K. V. Karabeshkin<sup>2</sup>,  
P. G. Gabdullin<sup>1</sup>, A. V. Arkhipov<sup>1</sup>*

<sup>1</sup> Peter the Great St. Petersburg Polytechnic University, St. Petersburg, Russia;

<sup>2</sup> Joint-Stock Company "Research and Production Enterprise "ELAR", St. Petersburg, Russia

✉ [arkhipov@rphf.spbstu.ru](mailto:arkhipov@rphf.spbstu.ru)

**Abstract.** This work continues the studies of low-threshold field electron emission from thin (6–10 nm) films of refractory metals (Mo or Zr) deposited on flat Si substrates. Now, we have investigated the changes in the films' morphology induced by thermo- and electroforming procedures and by the extraction of emission current. In SEM images of the samples taken after emission experiments, we observed the signs of solid-state dewetting (agglomeration) of the films, presumably caused by ion bombardment. This hypothesis was verified by SRIM simulations of the effect of ions on Mo-film/Si-substrate structure, as well as by an experiment at a HVEE-500 ion implanter.

**Keywords:** thin films, low-field electron emission, film dewetting, ion bombardment

**Funding:** The reported study was funded by Russian Science Foundation (Grant No. 23-29-10027; <https://rscf.ru/project/23-29-10027/>), and by St. Petersburg Science Foundation (Grant No. 23-29-10027).

**Citation:** Bizyaev I. S., Karaseov P. A., Karabeshkin K. V., Gabdullin P. G., Arkhipov A. V., Transformation of the structure of thin metal films upon activation of their ability to low-voltage electron emission, St. Petersburg State Polytechnical University Journal. Physics and Mathematics. 17 (2) (2024) 80–93. DOI: <https://doi.org/10.18721/JPM.17207>

This is an open access article under the CC BY-NC 4.0 license (<https://creativecommons.org/licenses/by-nc/4.0/>)



Научная статья  
УДК 537.533.2, 538.975, 539.1.06  
DOI: <https://doi.org/10.18721/JPM.17207>

## ТРАНСФОРМАЦИЯ СТРУКТУРЫ ТОНКИХ МЕТАЛЛИЧЕСКИХ ПЛЕНОК ПРИ АКТИВИРОВАНИИ ИХ СПОСОБНОСТИ К НИЗКОВОЛЬТНОЙ ЭМИССИИ ЭЛЕКТРОНОВ

И. С. Бизяев<sup>1</sup>, П. А. Карасев<sup>1</sup>, К. В. Карабешкин<sup>2</sup>  
П. Г. Габдуллин<sup>1</sup>, А. В. Архипов<sup>1</sup>✉

<sup>1</sup> Санкт-Петербургский политехнический университет Петра Великого, Санкт-Петербург, Россия;

<sup>2</sup> Акционерное общество «Научно–производственное предприятие «ЭЛАР»»,  
Санкт-Петербург, Россия

✉ [arkhipov@rphf.spbstu.ru](mailto:arkhipov@rphf.spbstu.ru)

**Аннотация.** Настоящая работа является продолжением исследований свойств низкопороговой автоэлектронной эмиссии из тонких (10 – 6 нм) пленок металлов Mo и Zr, сформированных на плоских подложках Si. Теперь изучались изменения морфологии пленок, вызываемые термополевым активированием и отбором эмиссионного тока. Основным экспериментальным методом была электронная микроскопия. Выдвинута гипотеза, что механизм указанных воздействий можно описать как твердотельный деветтинг (агломерация) покрытия, подвергнутого ионной бомбардировке. Для ее проверки средствами пакета SRIM проведено численное моделирование воздействия ионов на структуру Mo-пленка – Si-подложка, а также поставлен эксперимент с использованием ионного имплантера HVEE-500.

**Ключевые слова:** тонкая металлическая пленка, низковольтная эмиссия электронов, деветтинг пленки, ионная бомбардировка

**Финансирование:** Исследование поддержано средствами гранта Российского научного фонда № 23-29-10027 (<https://rscf.ru/project/23-29-10027/>) и гранта Санкт-Петербургского научного фонда № 23-29-10027.

**Ссылка для цитирования:** Бизяев И. С., Карасев П. А., Карабешкин К. В., Габдуллин П. Г., Архипов А. В. Трансформация структуры тонких металлических пленок при активировании их способности к низковольтной эмиссии электронов // Научно-технические ведомости СПбГПУ. Физико-математические науки. 2024. Т. 17. № 2. С. 80–93. DOI: <https://doi.org/10.18721/JPM.17207>

Статья открытого доступа, распространяемая по лицензии CC BY-NC 4.0 (<https://creativecommons.org/licenses/by-nc/4.0/>)

### Introduction

Many types of nanostructured materials and films are capable of emitting electrons at room temperature in moderate electric fields (several V/ $\mu\text{m}$  or less) [1–3]. This is unsurprising in carbon nanotubes, nanowalls, fibers and other similar structures capable of providing significant local geometric amplification of the applied field at the tips and edges. However, structures relatively smooth surfaces that do not contain morphological elements with a high geometric aspect ratio were also found to be capable of low-threshold cold emission [4–11]. In particular, we previously found that this property may be inherent in thin metal films, namely, molybdenum and zirconium films with the thickness ranging from 6 to 10 nm deposited on the surface of naturally oxidized silicon. The results of the experiments shedding light on the problem were presented in [12, 13]. In particular, it was reported that the threshold current of 100 nA/s can be extracted in samples of such films at the flat top of a cylindrical anode 6 mm in diameter (located 0.5–0.6 mm away from the sample) for macroscopic electric fields as low as of 1.8–6.4 V/ $\mu\text{m}$ . It was also observed

that the structure of the coating had to be partially transformed from initially solid to that containing nanoislands to stabilize the emission current. Thermal field (TF) treatment consisting of electroforming at elevated temperature was performed for this purpose.

This work focuses on the mechanism behind the transformation of the structure of emissive coatings due to TF treatment and/or prolonged extraction of emission current.

There is much interest in this phenomenon because of the potential applications of metal island films, for instance, in plasmonics and in thermoelectric converters.

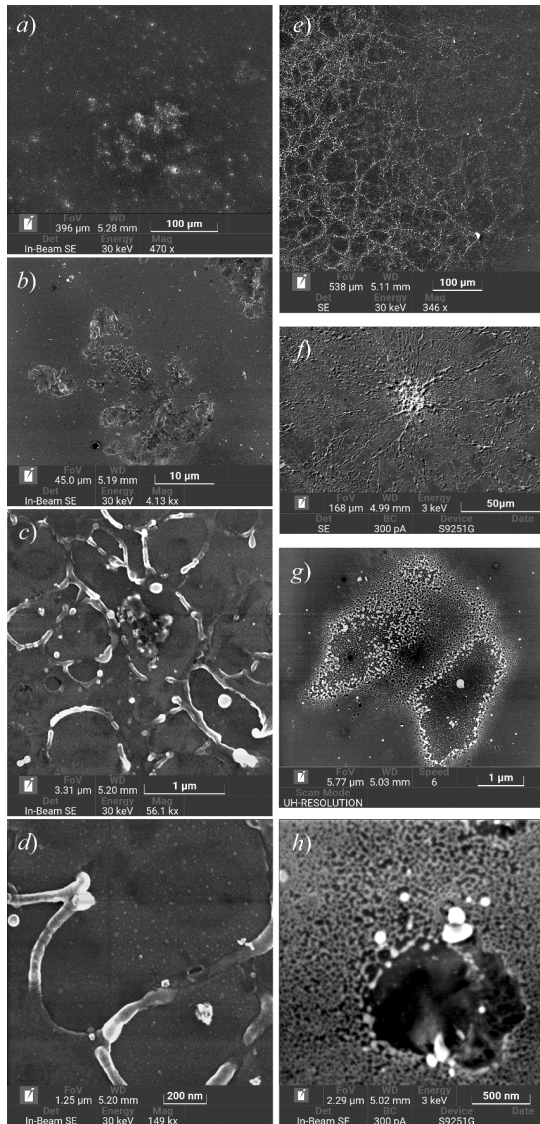


Fig. 1. Surface SEM images for 10 nm thick Mo film samples (a–d) and 8 nm thick Zr film samples (e–h) after emission experiments (scale bars correspond to different resolutions)

ments and consisted of grains with characteristic lateral dimensions of the order of tens of nanometers. One of these images (also presented in previous publications [12, 13]) is given below. The surface of the coatings from which the highest emission currents were extracted was considerably transformed after the emission experiments: regions with a modified (damaged) structure appeared, evidently acting as the centers of low-threshold cold electron emission. Different samples exhibited markedly different transformations.

### Experimental procedure

The studies were performed for the same metal film samples as in our earlier works [12, 13]. Magnetron sputtering was used to deposit molybdenum and zirconium films whose thickness ranged from 8 to 10 nm on naturally oxidized plates of KDB–10 grade monocrystalline silicon with *p*-type conductivity. A Mantis HEX system (Mantis Deposition, Thame, UK) was used for deposition; sputtering of the targets was carried out in argon atmosphere at a pressure of  $5 \cdot 10^{-3}$  mbar at a rate of about 0.1–1.0 E/s, the temperature of the substrates was 100–150 °C. The thickness of the deposited coatings was determined by a quartz balance.

Before the experiments to determine the capability for emission started, the samples were baked in vacuum for several hours for surface degassing. After that, the samples were subjected to electroforming or TF treatment at temperatures up to 600 °C. The emission characteristics were measured at room temperature and residual pressure of the order of  $10^{-9}$  mbar.

An HVEE 500 kV ion implanter was used in the experiment to simulate the effects of ion irradiation on the coating structure. The sample was irradiated with 10 keV fluorine ions at room temperature and/or at 500 °C.

In all cases, data on the structure of the films were obtained using scanning electron microscopes (SEM) manufactured by Tescan, Czech Republic (Mira, Lyra and Solaris models). The resulting images were processed using the Gwyddion program to eliminate technical defects and increase contrast.

### Experimental results and discussion

**Microscopic images of the surface.** Microscopic images of Mo and Zr films with an average thickness of 8 or 10 nm were obtained using the SEM method. Analysis of the films indicates that the coatings were solid prior to the emission experi-



Fig. 1, *a–d* shows surface images of the Mo film with the effective thickness of 10 nm yielding the best emission properties: the threshold macroscopic field strength (for a current of 100 nA) was  $1.8 \text{ V}/\mu\text{m}$  with the extracted stabilized current of the order of tens of  $\mu\text{A}$  for tens of hours [13]. Evidently, the main type of defects were circular, crater-like holes ranging in size from fractions to tens of  $\mu\text{m}$ , sometimes merging with each other. Comprehensive analysis of high-resolution SEM images (see Fig. 1, *c,d*) as well as data from X-ray microanalysis and atomic force microscopy confirmed that the amount of molybdenum inside the craters is reduced tenfold and the metal in these regions is preserved only as separate nanoscale-size islands. The craters are surrounded by elevated rims to which the coating material migrates. Notably, the redistribution of the material did not affect the substrate; its exposed regions remained flat.

The described reconstruction behavior of the metal coating (Fig. 1, *a–d*) was achieved for a Mo film sample yielding the best stable emission properties, which is why it was subjected to the longest emission tests with the highest extracted current. Somewhat different types of damage were accumulated in other samples under TF treatment, electroforming and current extraction.

As an example, Fig. 1, *e–h* shows SEM images for 8 nm thick Zr film, obtained after emission testing. The overview images (see Fig. 1, *e, f*) show an extensive network of coating regions containing line defects. Their fine structure can be seen in the images with the highest magnification (see Fig. 1, *g, h*). The same as in the case above, the process of morphological transformation of the film apparently began with the formation of submicron-sized holes (see Fig. 1, *h*). However, a slightly different picture was subsequently observed for the material from the vacated regions of the surface, composing relatively large (up to 100 nm) circular islands (see Fig. 1, *g*) rather than rims.

Noteworthy structures were also detected on the surfaces of several samples of metal films whose emission properties rapidly degraded during testing. Fig. 2, *a–c* shows SEM images of the regions of the 8 nm thick Mo film, Fig. 2, *d–f* those of the regions of the Zr film with the same thickness. The structures shown in the overview images *a, b, d* and *e* consist of several (4–6) relatively wide branches emanating from a common center. As evident from the SEM images, a fraction of the film material moved from the inside of each branch to the surrounding rim. The large-scale images in Fig. 2, *c, f* show a network of light lines, probably also corresponding to the line defects on the surface.

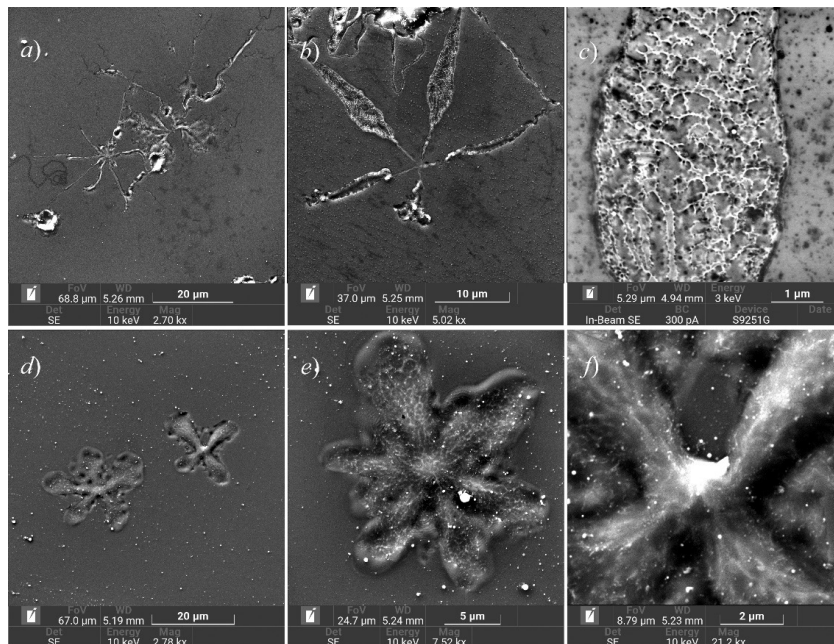


Fig. 2. Branched structures found in SEM images of Mo (*a–c*) and Zr (*d–e*) coatings (8 nm thick)

Images shown in panels *c* and *f* represent the same regions of the coatings as in *b* and *d*, but at a higher magnification

Thus, we can confirm that regions with modified morphology appeared in the initially solid thin-film samples due to the influence of factors associated with the activation of emission ability. Agglomeration of the films occurred in this case: the amount of coating material in some regions of the surface was significantly reduced due to its lateral transfer to other regions. In some cases, the film structure clearly started to contain islands in some regions (see Fig. 1 *d, g, h*), which may explain the ability to low-threshold cold electron emission observed in such samples [4, 9, 10].

**Mechanism of film agglomeration.** The SEM images obtained (see Figs. 1 and 2) combined with the findings from earlier studies using AFM and X-ray microanalysis [12, 13] indicate that the damage in the coatings occurred during emission experiments with metal films largely due to activated material transfer along the surface rather than due to its evaporation or atomization, which could be expected upon rapid local energy release, for example, during electrical breakdown.

The transformation of solid thin metal films into island ones due to lateral transfer of the material is known as solid-state dewetting (the term *agglomeration* is also used in Russian-language literature) [14–16]. When metal is deposited on a dielectric substrate (poorly wetting it), a solid coating can form at initial low temperatures due to low surface mobility of atoms. Such a coating is transformed into an island coating during subsequent thermal annealing, with temperatures significantly below the melting point of the metal generally required for this purpose. The cause of the dewetting phenomenon is the thermodynamic instability of films whose thicknesses range from units to tens of nanometers. This instability is due to the peculiarities of interatomic forces, specifically, the repulsive (short-range) and attractive (long-range) van der Waals forces [17]; or, in another formulation, the forces of diffusion and surface tension.

The general picture (see, for example, [14–18]) is that the dewetting process of a solid coating begins with the appearance of small holes (craters) whose number and size gradually increase. The coating material transferred from the hole forms elevated rims surrounding them. Next, the holes begin to come into contact, and the final coating structure is formed as a result of redistribution of the material in the rims. It can be different and depends on the parameters of the interaction of the atoms in the coating material with each other and with the substrate as well as on the annealing conditions. The formation of both large discrete particles, similar to those shown in Fig. 1, *g*, and branched (also called *web-like*) structures [15, 18]), similar to those shown in Fig. 1, *e, f* and Fig. 2, *b, d*, was previously described in the literature.

Thus, there is every reason to interpret the appearance of most types of defects in metal films subjected to TF treatment and emission experiments as dewetting occurring under the influence of factors related to extraction of the emission current. In particular, this interpretation allows to explain the correlation of the emission ability observed earlier (in experiments with carbon films [9, 10]) with the presence of a natural oxide layer on silicon substrates: the adhesion of coatings to silicon dioxide is typically lower than their adhesion to pure silicon surface, which can facilitate the transformation of the film structure during activation of their emission ability.

**Estimation of dewetting conditions.** Thus, an island film is the thermodynamically stable morphological shape for metal coatings up to several tens of nanometers thick deposited on dielectric substrates, since its free energy is lower than the free energy of a solid coating [14–16]. However, solid coatings are transformed into island coatings only at elevated temperatures, since this requires lateral atomic transfer with sufficiently high activation energies. The temperature at which dewetting can be observed depends on the material and thickness of the coating, as well as on the characteristics of the substrate.

Consider gold coatings whose quantitative patterns of dewetting are the best understood. For instance, the activation energy of dewetting was determined in [16] for gold coatings of different thicknesses on silicon nitride substrates. Its values were 1.04 eV for 15 nm thick films and 1.42 eV for 22 nm thick films. The observations were carried out in the temperature range from 300 to 600 °C, which is significantly below the melting point of gold (1064 °C).

The TF treatment aimed at activation of the emission ability of films in our experiments was also carried out at temperatures up to 600 °C. However, we considered metals with much higher melting points (their tabular values are 2623 °C for molybdenum and 1852 °C for zirconium).

Notably, there are scarce data in the literature on dewetting in molybdenum or zirconium films. A significant study [18] observed the process of agglomeration in a 20 nm thick Mo coating deposited on a sapphire substrate. The dewetting of this coating occurred within tens or hundreds of minutes, which approximately corresponds to the duration of the TF treatment in our studies.



However, the samples in [18] were heated to a temperature of 940 °C, significantly higher than the values that we used. This observation is in good agreement with the fact that Mo films exhibited no morphological transformations outside the «projection» of the anode in the region where the only factor influencing the film was the elevated temperature, while the influence of the electric field and the factors associated with extraction of emission current was excluded (this is discussed in our earlier paper [13]). The specific local influence of these factors might have been the reason for the observed local transformation of the film structure and activation of their emission ability.

It was found [19–23] that the dewetting process can be stimulated not only by heating the sample, but also by optical, electronic or ion irradiation (induced by local heating). Estimates of the expected effectiveness of such local contributors are given below for experimental conditions described in [12, 13].

Let us evaluate the temperature of local Joule heat released from the flow of emission current through the emission centers. TF treatment of the samples in [12, 13] was carried out with the extracted emission current  $I = 100 \text{ nA} = 10^{-7} \text{ A}$ . Suppose that as current flows through the emission center, each electron transfers energy of the order  $\Delta E = 1 \text{ eV}$  to heat (this assumption is substantiated in [24]). The power of such a heat source is  $P = I \cdot \Delta E / e = 10^{-7} \text{ W} = 100 \text{ nW}$ . An initial estimate of the temperature drop  $\Delta T$  produced by this source can be obtained by solving the simple problem on the propagation of a stationary heat flow from a local surface source of size  $d$  into a thick silicon wafer (with the thermal conductivity  $\kappa = 148 \text{ W/(m}\cdot\text{K)}$ ). The result of the solution is

$$\Delta T \approx \frac{P}{2\pi\kappa d}. \quad (1)$$

If we select the typical size of the observed craters  $d = 1 \text{ }\mu\text{m}$  as the size of the heat release region, we obtain a negligible value for estimating the temperature increment:  $\Delta T \approx 10^{-4} \text{ K}$ . Apparently, the local temperature increment remains insignificant, amounting to  $\Delta T \approx 0.01 \text{ K}$ , even for the smallest possible size of the heat release region  $d = 10 \text{ nm}$  (the order of size of individual nanostructures detectable in microscopic images in Fig. 1,  $d$  and  $h$ ).

However, the above evaluation ignores the specifics of nanoscale heat transfer processes, where the contribution from the interface between the media to the total thermal resistance of structures turns out to be predominant [25]. If at least one of the contacting media is not a metal and heat is transferred mainly by phonons, each interface is characterized by the so-called Kapitza resistance  $R_K$  [26]. This parameter relates the interfacial temperature drop to the heat flux  $q$ :  $\Delta T = R_K \cdot q$ . In effect, it turns out [25, 27, 28] that the value of the Kapitza resistance for most practically interesting cases lies in a relatively narrow range:

$$R_K = (0.6 - 3.0) \cdot 10^{-8} \text{ m}^2 \cdot \text{K/W}.$$

The maximum estimate of  $\Delta T$  is obtained taking the value of  $R_K$  at the right endpoint of the given range and setting the smallest size of the heat release region:  $d = 10 \text{ nm}$ .

Estimating the heat flux across the boundary as  $q = P/d^2$ , we obtain that

$$\Delta T = R_K \cdot P/d^2 \approx 30 \text{ K}.$$

This value still seems insufficient for explaining the observed transformations in the morphology of the coatings.

The above estimates indicate that local heating of the sample surface induced by the flow of emission current cannot activate the film dewetting process to a sufficient extent.

Let us consider the scenario when the activating factor was the bombardment of the coating regions adjacent to the emission center with ions formed by ionization of residual gas by the emitted electron current. Fig. 3 shows a schematic representation of the experimental device used for TF treatment of samples and measurement of emission current–voltage characteristics.

Let us again set the value of the emission current  $I = 100 \text{ nA}$ . The concentration of neutral molecules in the field gap,  $n$ , can be estimated based on the residual gas pressure of  $10^{-8} \text{ Torr}$  (it may be higher than in other parts of the experimental device), which corresponds to  $n \approx 3.6 \cdot 10^{14} \text{ m}^{-3}$ . Generally speaking, the ionization cross section of gas molecules by electron impact depends on

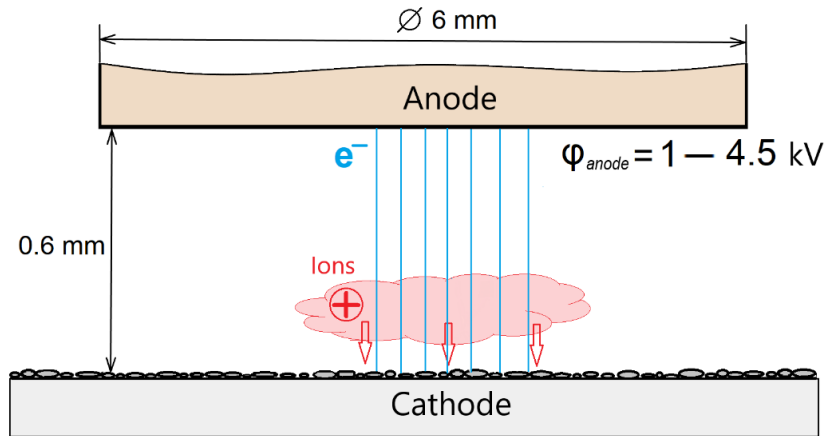


Fig. 3. Schematic of field gap of experimental device

The region colored in pink is where the energy of the emitted electron current (blue lines) reaches the maximum ionization cross section of residual gas and where the largest number of ions (+) bombarding the sample surface are produced (the direction of bombardment is shown by arrows)

the type of gas and on the electron energy of the electrons, varying as they move in the field gap (see Fig. 3). We choose the value of the cross section  $\sigma = 10^{-20} \text{ m}^2$  as an averaged estimate. The width of the field gap in the experiments was  $h = 0.6 \text{ mm}$ . In view of this, the ion current  $I_i$  can be written as

$$I_i = I \cdot n \sigma h \approx 2 \cdot 10^{-15} \text{ A.}$$

Next, we estimate the ion beam fluence  $D$  for time  $t = 1000 \text{ s}$ , corresponding in order of magnitude to the typical duration of the TF treatment procedure. We assume that the ion current is distributed over an area  $S = 1 \text{ }\mu\text{m}^2 = 10^{-12} \text{ m}^2$  (this is the area of a typical crater in microscopic images, see Fig. 1, *c*, *d* and *h*). We obtain:

$$D = \frac{I_i t}{e S} \approx 10^{18} \text{ m}^{-2} = 10^{14} \text{ cm}^{-2}. \quad (2)$$

This value can be compared with the literature data on ion beam fluences sufficient for initiating dewetting in metal films. For example, a transformation (caused by ion irradiation) of a solid gold film deposited on monocrystalline silicon was observed in [23]; the solid film was transformed into a coating consisting of discrete islands with the lateral size of the order of tens of micrometers. This transformation required irradiation with a fluence in the range  $(4.0-9.5) \cdot 10^{13} \text{ cm}^{-2}$ , which is comparable to estimate (2).

Notably, however, there are several significant differences in the conditions of the compared experiments. The sample considered in [23] was a 1.5 nm thick gold film, while our experiments were carried out with more refractory metals and with coatings of greater thickness. These two differences would be expected to increase the activation energy of atomic migration on the surface. On the other hand,  $\text{PF}_4^+$ ,  $\text{BF}_2^+$  and  $\text{Ta}^{4+}$  ions with sufficiently high energy (0.65 keV/u) were used in [23], typically penetrating deep into the samples. This can weaken the activating effect of radiation on surface migration. The nature of the coating materials seems to be the most significant among these factors; unfortunately, we were unable to uncover any data on the effect of ion irradiation on dewetting of molybdenum and zirconium films in the literature. For this reason, we decided to conduct an additional experiment to directly observe the effect of ion irradiation on one of the film samples whose properties were studied in this paper and earlier in [12, 13].

### Effects of ion irradiation: experiment and simulation

**Experimental** The effect of ion irradiation on the morphology of a Mo film was studied based on the experiment with a sample of 10 nm thick Mo coating on a KDB-10 grade silicon plate.



The peripheral part of the film was used for irradiation and microscopic studies, laying outside the region to which the electric field was applied during the earlier emission testing and therefore not contributing to the emission current.

At the first stage of the experiment, two sections of the sample were exposed to ion irradiation with a fluence (dose) of  $10^{12}$  and  $10^{13}$   $\text{cm}^{-2}$  at room temperature. Fluorine ions whose mass is close to atomic masses of atmospheric gases were used. The ion energy was equal to 10 keV, i.e., the minimum value technically achievable for implantation system used. After morphological control of the irradiated and non-irradiated parts of the coating, the sample was reloaded into the implanter and irradiated with the same ions for a second time, but at a dose of  $10^{14}$   $\text{cm}^{-2}$  and at a temperature of 500 °C.

Fig. 4 shows images of the sample surface before and after irradiation with doses of  $10^{13}$  and  $10^{14}$   $\text{cm}^{-2}$ . The brightest points in the images correspond to defects produced due to prolonged irradiation of the surface by a stopped scanning electron beam.

Even though the maximum fluence was equal to the calculated value (from Eq. (2)), no signs of coating dewetting could be detected in the SEM images. The only transformation observed is in the structure of the grains whose boundaries are practically absent in Fig. 4,c, obtained after

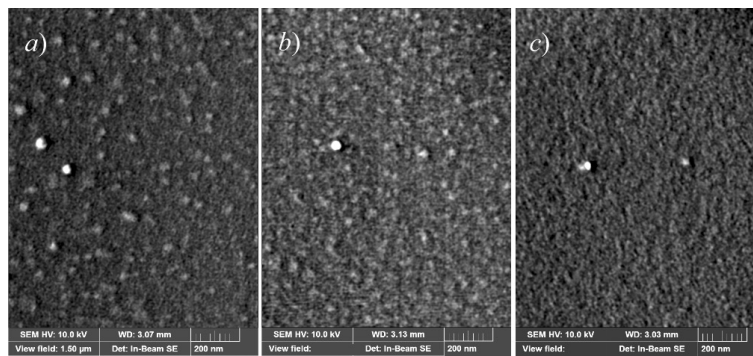


Fig. 4. Surface SEM images for 10 nm thick Mo coating sample obtained at 23 °C before ( $D = 0$ ) (a) and after ( $D > 0$ ) single (b) and double (c) irradiation with 10 keV  $F^+$  ions with different fluences  $D$ ,  $\text{cm}^{-2}$ :  $10^{13}$  (b);  $10^{13}$  (23 °C) +  $10^{14}$  (500 °C) (c)

irradiation with the highest ion fluence, which can be interpreted as a sign of amorphization of the coating.

Coating dewetting at such a fluence value occurred in the experiments with films of more fusible gold [23], even in the case of irradiation at room temperature. On the other hand, the studies in [23] also found that the smoothing of the surface of the gold film at relatively small irradiation doses precedes the period when the film starts to break into islands. This suggests that coating dewetting could also be achieved with a further increase in the dose in our experiment with the implanter.

A significant difference (for the dewetting process) between the ion bombardment accompanying the extraction of the emission current and that in the experiment with the implanter is possibly in the lower average ion energy in the first case, which should lead to a difference in the penetration depth of these ions into the sample.

The maximum ion energy in the emission experiments was determined by the magnitude of the voltage applied to the field gap, which did not exceed 4.5 kV. As for samples with the best emission ability, this voltage did not exceed 1 kV [12, 13]. The average ion energy could be even lower: a wide energy distribution from zero to the value corresponding to the anode potential can be expected for ions produced due to ionization of the residual gas by electron impact (see Fig. 3).

**Numerical simulation** To confirm the possible role of the voltage factor applied to the field gap, we carried out numerical simulation of the interaction between the ions normally incident on 8 nm thick Mo film on silicon substrate and this structure. The standard SRIM package which is the most widespread for simulations of ion implantation was used. The threshold displacement energies were assumed to be 25 and 15 eV for molybdenum and silicon atoms, respectively. To reduce the statistical error, 15,000 independent cases were simulated. The simulation results are shown in Fig. 5.

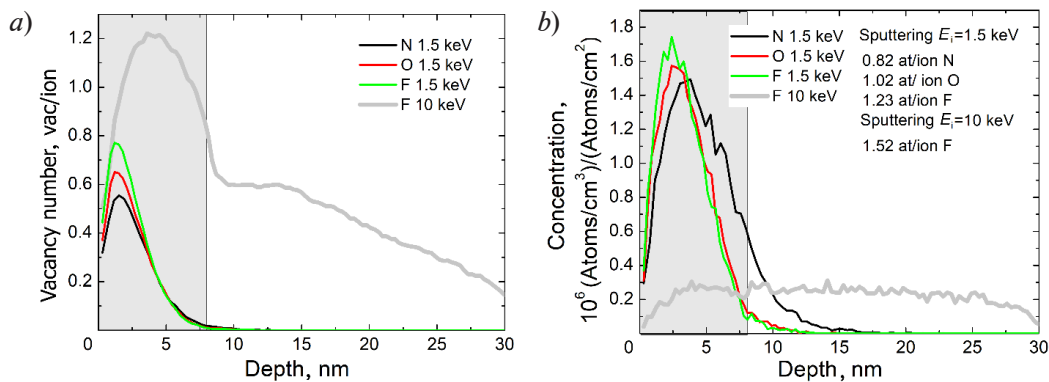


Fig. 5. Calculated distributions of defects produced per ion over target depth (a) and concentrations of injected impurity (b) in Mo (8 nm)-Si structure during bombardment with different ions (given in the legend)

According to the calculation results, 10 keV ions corresponding to the conditions of the implanter experiment penetrate all the way through the Mo film and a significant number of defects are produced in the surface layer of the silicon substrate. This should adversely affect the coating dewetting process, contributing to mutual diffusion of the film materials, the substrate and the silicon dioxide layer separating them. However, in the case of 1.5 keV ions, it is only the coating that is mostly exposed to them, while the interface with the substrate is virtually unaffected. Therefore, the ion beam bombarding the surface of the samples during TF treatment and emission current extraction in our experiments described in [12, 13] could more effectively stimulate the dewetting process, transferring additional energy to the coating atoms and contributing to an increase in their surface mobility.

The proposed explanation should not be considered as the only possible one. For example, it is known that the action of the electric field itself can increase the surface mobility of atoms and cause agglomeration of films [15]. Studies on electron emission in current flow along thin metal films (see, for example, [29]) interpreted the activating effect of electroforming on coatings precisely as the increase in atomic mobility in a strong electric field. Another potential activating factor is the excitation of electrons in the atomic outer shells by direct action of the electron emission current; this phenomenon of film agglomeration electron irradiation was also described in the literature [19, 20].

### Conclusion

The paper analyzes microscopic surface images of thin molybdenum and zirconium film samples, both initially solid and after their thermal field treatment consisting of applying an electric field and extracting an emission current under heating to a predetermined temperature (no higher than 600 °C). The samples subjected to this procedure exhibited (to a greater or lesser extent) cold electron emission in a low-intensity macroscopic electric field (on the order of several V/ $\mu$ m). It was found that the best emission properties of 10 nm thick molybdenum films correlate with a certain type of transformation of their surface during treatment and current extraction, i.e., holes evolving in the film, inside which the coating metal is present as isolated nanoislands. Regions of a different structure appeared during treatment and current extraction in the samples exhibiting the worst emission parameters (in particular, in 8 nm thick molybdenum and zirconium films). The results of image analysis, numerical estimates, simulation and additional experiments indicate that the transformation of the coating structure occurred by the mechanism of solid-state dewetting stimulated by ion bombardment. This opens up the possibilities for developing ion-beam technologies aimed at synthesis of effective emission or thermoelectric structures based on arrays of metal islands.



## REFERENCES

1. **Fursey G. N.**, Field emission in vacuum microelectronics, Kluwer Academic–Plenum Publishers, New York, USA, 2005.
2. **Evtukh A., Hartnagel H., Yilmazoglu O., et al.**, Vacuum nanoelectronic devices: Novel electron sources and applications, John Wiley & Sons, Hoboken, USA, 2015.
3. **Egorov N. V., Sheshin E. P.**, Field emission electronics, Springer, Berlin, Germany, 2017.
4. **Eidelman E. D., Arkhipov A. V.**, Field emission from carbon nanostructures: Models and experiment, *Phys.–Usp.* 63 (7) (2020) 648–667.
5. **Bandurin D. A., Mingels S., Kleshch V. I., et al.**, Field emission spectroscopy evidence for dual-barrier electron tunnelling in nanographite, *Appl. Phys. Lett.* 106 (23) (2015) 233112.
6. **Fursey G. N., Polyakov M. A., Bagraev N. T., et al.**, Low-threshold field emission from carbon structures, *J. Surf. Invest.: X-Ray, Synchrotr. Neutron Tech.* 13 (5) (2019) 814–824.
7. **Davidovich M. V., Yafarov R. K.**, Pulsed and static field emission VAC of carbon nanocluster structures: Experiment and its interpretation, *Tech. Phys.* 64 (8) (2019) 1210–1220.
8. **Streletskiy O. A., Zavidovskiy I. A., Nishchak O. Y., et al.**, Low-threshold field emission cathode based on heat-treated dehydrofluorinated polyvinylidene fluoride, *JETP.* 135 (6) (2022) 844–852.
9. **Andronov A., Budylna E., Shkitun P., et al.**, Characterization of thin carbon films capable of low-field electron emission, *J. Vac. Sci. Technol. B.* 36 (2) (2018) 02C108.
10. **Gabdullin P., Zhurkin A., Osipov V., et al.**, Thin carbon films: Correlation between morphology and field-emission capability, *Diam. Relat. Mater.* 105 (May) (2020) 107805.
11. **Smerdov R., Mustafaev A.**, Novel low-macroscopic-field emission cathodes for electron probe spectroscopy systems, *J. Appl. Phys.* 134 (11) (2023) 114903.
12. **Bizyaev I. S., Gabdullin P. G., Gnuchev N. M., Arkhipov A. V.**, Low-field electron emission from thin films of metals, *St. Petersburg State Polytechnical University Journal. Physics and Mathematics.* 14 (1) (2021) 105–120.
13. **Bizyaev I., Gabdullin P., Chumak M., et al.**, Low-field electron emission capability of thin films on flat silicon substrates: Experiments with Mo and general model for refractory metals and carbon, *Nanomaterials.* 11 (12) (2021) 3350.
14. **Thompson C. V.**, Solid-state dewetting of thin films, *Annu. Rev. Mater. Res.* 42 (1) (2012) 399–434.
15. **Altomare M., Nguyen N. T., Schmuki P.**, Templated dewetting: designing entirely selforganized platforms for photocatalysis, *Chem. Sci.* 7 (12) (2016) 6865–6886.
16. **Niekil F., Schweizer P., Kraschewski S. M., et al.**, The process of solid-state dewetting of Au thin films studied by in situ scanning transmission electron microscopy, *Acta Mater.* 90 (15 May) (2015) 118–132.
17. **Sharma A., Khanna R.**, Pattern formation in unstable thin liquid films, *Phys. Rev. Lett.* 81 (16) (1998) 3463–3466.
18. **Kovalenko O., Szaby S., Klinger L., Rabkin E.**, Solid state dewetting of polycrystalline Mo film on sapphire, *Acta Mater.* 139 (15 Oct) (2017) 51–61.
19. **Kojima Y., Kato T.**, Nanoparticle formation in Au thin films by electron-beam-induced dewetting, *Nanotechnology.* 19 (25) (2008) 255605.
20. **Ruffino F., Grimaldi G.**, Controlled dewetting as fabrication and patterning strategy for metal nanostructures, *Phys. Status Solidi A.* 212 (8) (2015) 1662–1684.
21. **Lian J., Wang L., Sun X., et al.**, Patterning metallic nanostructures by ion-beam-induced dewetting and Rayleigh instability, *Nano Lett.* 6 (5) (2006) 1047–1052.
22. **Savio R. L., Repetto L., Guida P., et al.**, Control of the micrometric scale morphology of silicon nanowires through ion irradiation-induced metal dewetting, *Solid State Commun.* 240 (Aug) (2016) 41–45.
23. **Tuzhilkin M. S., Bepalova P. G., Mishin M. V., et al.**, Formation of Au nanoparticles and features of etching of a Si substrate under irradiation with atomic and molecular ions, *Semiconduct.* 54 (1) (2020) 137–143.
24. **Arkhipov A. V., Eidelman E. D., Zhurkin A. M., et al.**, Low-field electron emission from carbon cluster films: Combined thermoelectric/hot-electron model of the phenomenon, *Fuller. Nanotub. Car. N.* 28 (4) (2020) 286–294.
25. **Cahill D. G., Ford W. K., Goodson K. E., et al.**, Nanoscale thermal transport, *J. Appl. Phys.* 93 (2) (2003) 793–818.

26. **Khalatnikov I. M.**, An introduction to the theory of superfluidity, Perseus Publishing, Cambridge, MA, 2000.
27. **Stoner R. J., Maris H. J.**, Kapitza conductance and heat flow between solids at temperatures from 50 to 300 K, *Phys. Rev. B.* 48 (22) (1993) 16373–16387.
28. **Meilakhs A. P.**, Nonequilibrium distribution function in the presence of a heat flux at the interface between two crystals, *Phys. Solid State.* 57 (1) (2015) 148–152.
29. **Fedorovich R. D., Naumovets A. G., Tomchuk P. M.**, Electron and light emission from island metal films and generation of hot electrons in nanoparticles, *Phys. Rep.* 328 (2–3) (2000) 73–179.

## СПИСОК ЛИТЕРАТУРЫ

1. **Fursey G. N.** Field emission in vacuum microelectronics. New York: Kluwer Academic Plenum Publishers, 2005. 205 p.
2. **Evtukh A., Hartnagel H., Yilmazoglu O., Mimura H., Pavlidis D.** Vacuum nanoelectronic devices: Novel electron sources and applications, Hoboken, USA: John Wiley & Sons, 2015. 453 p.
3. **Шешин Е. П., Егоров Н. В.** Автоэлектронная эмиссия. Принципы и приборы. М.: ИД «Интеллект», 2011. 704 с.
4. **Эйдельман Е. Д., Архипов А. В.** Полевая эмиссия из углеродных наноструктур: модели и эксперимент // *Успехи физических наук.* 2020. Т. 190. № 7. С. 693–714.
5. **Bandurina D. A., Mingels S., Kleshch V. I., Luetzenkirchen-Hecht D., Mueller G., Obraztsov A. N.** Field emission spectroscopy evidence for dual-barrier electron tunnelling in nanographite // *Applied Physics Letters.* 2015. Vol. 106. No. 23. P. 233112.
6. **Фурсей Г. Н., Поляков М. А., Баграев Н. Т., Закиров И. И., Нашекин А. В., Бочаров В. Н.** Низкопороговая полевая эмиссия из углеродных структур // *Поверхность. Рентгеновские, синхротронные и нейтронные исследования.* 2019. № 9. С. 28–39.
7. **Давидович М. В., Яфаров Р. К.** Импульсные и статические автоэмиссионные ВАХ углеродных нанокластерных структур: эксперимент и его интерпретация // *Журнал технической физики.* 2019. Т. 8 № .89. С. 1293–1282.
8. **Стрелецкий О. А., Завидовский И. А., Нищак О. Ю., Хайдаров А. А., Савченко Н. Ф., Павликов А. В.** Низкопороговый автоэмиссионный катод на основе термически обработанного дегидрофторированного поливинилиденфторида // *Журнал экспериментальной и теоретической физики.* 2022. Т. 162. № 6. С. 881–891.
9. **Andronov A., Budylna E., Shkitun P., Gabdullin P., Gnuchev N., Kvashenkina O., Arkhipov A.** Characterization of thin carbon films capable of low-field electron emission // *Journal of Vacuum Science & Technology B.* 2018. Vol. 36. No. 2. P. 02C108.
10. **Gabdullin P., Zhurkin A., Osipov V., Besedina N., Kvashenkina O., Arkhipov A.** Thin carbon films: Correlation between morphology and field-emission capability // *Diamond & Related Materials.* 2020. Vol. 105. May. P. 107805.
11. **Smerdov R., Mustafaev A.** Novel low-macroscopic-field emission cathodes for electron probe spectroscopy systems // *Journal of Applied Physics.* 2023. Vol. 134. No. 11. P. 114903.
12. **Бизяев И. С., Габдуллин П. Г., Гнучев Н. М., Архипов А. В.** Низкопороговая полевая эмиссия электронов тонкими металлическими пленками: связь эмиссионной способности с составом, условиями нанесения и морфологией // *Научно-технические ведомости СПбГПУ. Физико-математические науки.* 2021. Т. 14. № 1. С. 111–127.
13. **Bizyaev I., Gabdullin P., Chumak M., Babyuk V., Davydov S., Osipov V., Kuznetsov A., Kvashenkina O., Arkhipov A.** Low-field electron emission capability of thin films on flat silicon substrates: Experiments with Mo and general model for refractory metals and carbon // *Nanomaterials.* 2021. Vol. 11. No. 12. P. 3350.
14. **Thompson C. V.** Solid-state dewetting of thin films // *Annual Review of Materials Research.* 2012. Vol. 42. No. 1. Pp. 399–434.
15. **Altomare M., Nguyen N. T., Schmuki P.** Templated dewetting: designing entirely selforganized platforms for photocatalysis // *Chemical Science.* 2016. Vol. 7. No. 12. Pp. 6865–6886.
16. **Niekil F., Schweizer P., Kraschewski S. M., Butz B., Spiecker E.** The process of solid-state dewetting of Au thin films studied by in situ scanning transmission electron microscopy // *Acta Materialia.* 2015. Vol. 90. 15 May. Pp. 118–132.



17. **Sharma A., Khanna R.** Pattern formation in unstable thin liquid films // *Physical Review Letters*. 1998. Vol. 81. No. 16. Pp. 3463–3466.
18. **Kovalenko O., Szaby S., Klinger L., Rabkin E.** Solid state dewetting of polycrystalline Mo film on sapphire // *Acta Materialia*. 2017. Vol. 139. 15 Oct. Pp. 51–61.
19. **Kojima Y., Kato T.** Nanoparticle formation in Au thin films by electron-beam-induced dewetting // *Nanotechnology*. 2008. Vol. 19. No. 25. P. 255605.
20. **Ruffino F., Grimaldi G.** Controlled dewetting as fabrication and patterning strategy for metal nanostructures // *Physica Status Solidi A*. 2015. Vol. 212. No. 8. Pp.1662–1684.
21. **Lian J. Wang L., Sun X., Yu Q., Ewing R. C.** Patterning metallic nanostructures by ion-beam-induced dewetting and Rayleigh instability // *Nano Letters*. 2006. Vol. 6. No. 5. Pp. 1047–1052.
22. **Savio R. L., Repetto L., Guida P., Angeli E., Firpo G., Volpe A., Ierardi V., Valbusa U.** Control of the micrometric scale morphology of silicon nanowires through ion irradiation-induced metal dewetting // *Solid State Communications*. 2016. Vol. 240. August. Pp. 41–45.
23. **Тужилкин М. С., Беспалова П. Г., Мишин М. В., Колесников И. Е., Карабешкин К. В., Карасев П. А., Титов А. И.** Формирование наночастиц Au и особенности травления подложки Si после облучения атомарными и молекулярными ионами // *Физика и техника полупроводников*. 2020. Т. 54. № 1. С. 90–96.
24. **Arkhipov A. V., Eidelman E. D., Zhurkin A. M., Osipov V. S., Gabdullin P. G.** Low-field electron emission from carbon cluster films: Combined thermoelectric/hot-electron model of the phenomenon // *Fullerenes, Nanotubes and Carbon Nanostructures*. 2020. Vol. 28. No. 4. Pp. 286–294.
25. **Cahill D. G., Ford W. K., Goodson K. E., Mahan G. D., Majumdar A., Maris H. J., Merlin R., Phillpot S. R.** Nanoscale thermal transport // *Journal of Applied Physics*. 2003. Vol. 93. No. 2. Pp. 793–818.
26. **Халатников И. М.** Введение в теорию сверхтекучести. М.: Наука, 1965. 158 с.
27. **Stoner R. J., Maris H. J.** Kapitza conductance and heat flow between solids at temperatures from 50 to 300 K // *Physical Review B*. 1993. Vol. 48. No. 22. Pp. 16373–16387.
28. **Мейлахс А.П.** Неравновесная функция распределения при тепловом потоке вблизи границы двух кристаллов // *Физика твердого тела*. 2015. Т. 57. № 1. С. 140–144.
29. **Fedorovich R. D., Naumovets A. G., Tomchuk P. M.** Electron and light emission from island metal films and generation of hot electrons in nanoparticles // *Physics Reports*. 2000. Vol. 328. No. 2–3. Pp. 73–179.

## THE AUTHORS

**BIZYAEV Ivan S.**

*Peter the Great St. Petersburg Polytechnic University*  
29 Politechnicheskaya St., St. Petersburg, 195251, Russia  
ivanbiziaev@yandex.com  
ORCID: 0009-0005-7265-1173

**KARASEOV Platon A.**

*Peter the Great St. Petersburg Polytechnic University*  
29 Politechnicheskaya St., St. Petersburg, 195251, Russia  
platon.karaseov@spbstu.ru  
ORCID: 0000-0003-2511-0188

**KARABESHKIN Konstantin V.**

*Joint-Stock Company "Research and Production Enterprise «ELAR»"*  
68 Torez Ave., St. Petersburg, 194223, Russia  
yanikolaus@yandex.ru  
ORCID: 0000-0003-1770-1877

**GABDULLIN Pavel G.**

*Peter the Great St. Petersburg Polytechnic University*  
29 Politechnicheskaya St., St. Petersburg, 195251, Russia  
gabdullin\_pg@spbstu.ru  
ORCID: 0000-0002-2519-2577

**ARKHIPOV Alexander V.**

*Peter the Great St. Petersburg Polytechnic University*  
29 Politechnicheskaya St., St. Petersburg, 195251, Russia  
arkhipov@rphf.spbstu.ru  
ORCID: 0000-0002-3321-7797

**СВЕДЕНИЯ ОБ АВТОРАХ**

**БИЗИЯЕВ Иван Сергеевич** – аспирант Высшей инженерно-физической школы Санкт-Петербургского политехнического университета Петра Великого, научный сотрудник лаборатории «Самоорганизующиеся высокотемпературные наноструктуры» Санкт-Петербургского политехнического университета Петра Великого.

195251, Россия, г. Санкт-Петербург, Политехническая ул., 29  
ivanbiziaev@yandex.com  
ORCID: 0009-0005-7265-1173

**КАРАСЕВ Платон Александрович** – доктор физико-математических наук, профессор Высшей инженерно-физической школы Санкт-Петербургского политехнического университета Петра Великого.

195251, Россия, г. Санкт-Петербург, Политехническая ул., 29  
platon.karaseov@spbstu.ru  
ORCID: 0000-0003-2511-0188

**КАРАБЕШКИН Константин Валерьевич** – кандидат физико-математических наук, инженер Акционерного общества «Научно-производственное предприятие «ЭЛАР»».

194223, Россия, г. Санкт-Петербург, пр. Тореза, 68, лит. А  
yanikolaus@yandex.ru  
ORCID: 0000-0003-1770-1877

**ГАБДУЛЛИН Павел Гарифович** – кандидат физико-математических наук, доцент Высшей инженерно-физической школы Санкт-Петербургского политехнического университета Петра Великого.

195251, Россия, г. Санкт-Петербург, Политехническая ул., 29  
gabdullin\_pg@spbstu.ru  
ORCID: 0000-0002-2519-2577

**АРХИПОВ Александр Викторович** – доктор физико-математических наук, профессор Высшей инженерно-физической школы Санкт-Петербургского политехнического университета Петра Великого.

195251, Россия, г. Санкт-Петербург, Политехническая ул., 29  
arkhipov@rphf.spbstu.ru  
ORCID: 0000-0002-3321-7797

*Received 21.01.2024. Approved after reviewing 11.02.2024. Accepted 11.02.2024.*

*Статья поступила в редакцию 21.01.2024. Одобрена после рецензирования 11.02.2024. Принята 11.02.2024.*